

## **POINT DEFECTS IN FeAl**

Gary S. Collins and Luke S.J. Peng

Department of Physics,  
Washington State University,  
Pullman, Washington 99164-2814  
USA

### **ABSTRACT**

Point defects in annealed B2-phase FeAl samples in the range 47-53 at.% Fe were studied using  $^{57}\text{Fe}$  Mössbauer spectroscopy. Spectra were analyzed using local environment models according to which point defects in atomic shells close to probe atoms induce shifts in the nuclear monopole interaction. For well-annealed samples, better results were obtained assuming only the presence of  $\text{Fe}_{\text{Al}}$  antisite and  $\text{V}_{\text{Fe}}$  vacancy defects, and not of  $\text{Al}_{\text{Fe}}$  antisite defects.. Monopole interactions of  $^{57}\text{Fe}$  probes on the Fe and Al sublattices having no defects in the first two shells were about  $+0.27$  and  $-0.03$   $\text{mm s}^{-1}$ , respectively, with respect to Fe in alpha-Fe metal. The shifts induced by  $\text{Fe}_{\text{Al}}$  and  $\text{V}_{\text{Fe}}$  defects in the first shells of Fe probes on the Fe and Al sublattices were  $-0.134$  and  $-0.31$   $\text{mm s}^{-1}$ , respectively, and, in the second shells,  $+0.06$  and  $+0.086$   $\text{mm s}^{-1}$ . In addition to structural defects needed to accommodate deviations from stoichiometry, annealed samples were found to contain several percents of  $\text{Fe}_{\text{Al}}$  and  $\text{V}_{\text{Fe}}$  defects due to lattice disorder, with greater disorder in Fe-deficient alloys.

### **Introduction**

FeAl belongs to a class of ordered B2 (CsCl-structure) alloys formed from transition-metal (T) and trivalent elements that have wide phase ranges and are under investigation for applications as high-temperature structural materials. In these compounds, deviations from stoichiometry are accommodated by T-metal vacancies in T-deficient alloys and by T-metal antisite atoms in T-rich alloys. However, additional point-defect disorder has

been observed even in well-annealed samples of FeAl, for example by x-ray diffraction.[1] Such disorder is a consequence of a low enthalpy of formation of thermal defects and a high enthalpy of migration of vacancies, making it difficult to reach thermal equilibrium at low temperature. In FeAl the disorder is believed to involve the same defects that accomodate deviations from stiochiometry, that is, Fe-vacancies,  $V_{Fe}$ , and Fe-antisite atoms,  $Fe_{Al}$ . [1] This kind of disorder is shown schematically for a stoichiometric crystal in Fig.1, where two  $Fe_{Al}$  antisite atoms are observed to be compensated by four  $V_{Fe}$  vacancies. Other elementary point defects that have not been reported for annealed samples include the Al-antisite atom,  $Al_{Fe}$ , and Al-vacancy,  $V_{Al}$ . In the present work, we apply  $^{57}Fe$  Mössbauer spectroscopy to study the point defects by resolving different defects through the hyperfine interactions they induce at neighboring host atoms. The measurements encompass well-annealed samples having 47 to 53 atomic percent of Fe. In practice, the measured transmission spectra exhibited only a broadened absorption dip but, as will be shown below, the spectra can be satisfactorily fitted to obtain the defect concentrations using a local environment model. We obtain shifts in the monopole interactions at  $^{57}Fe$  probe atoms on both sublattices due to defects in the first two neighbor shells. In the future, we plan to use the measured shifts to determine point defect concentrations in quenched and mechanically-milled FeAl samples.

### Experiments

FeAl samples were made from metals of purity greater than 99.99% by arc-melting under argon and splat-quenching, yielding brittle foil fragments. Previous experience melting together NiAl and CoAl samples using the same arc-melter leads us to conclude that nominal compositions should be close to the actual ones and that sample homogeneity should be good.[2] Samples were ordered as well as possible by annealing at 430 C in air for five days, like the procedure used in a recent x-ray study.[1]

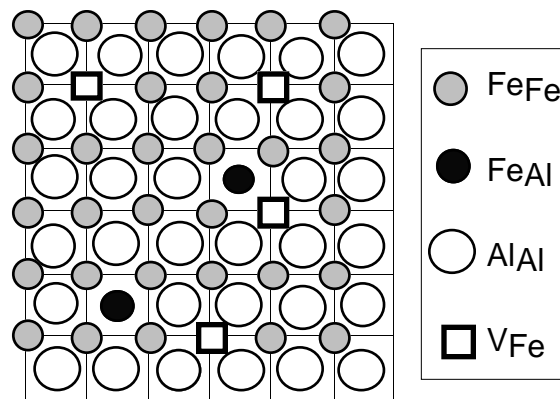


*Figure 1. Schematic of defects and local environments in FeAl.*

Mössbauer measurements were made in transmission geometry at room temperature using a single line source of  $^{57}\text{Co}$  in Pd. The zero-absorber-thickness extrapolated linewidth of the source was independently measured to be  $0.255 \text{ mm s}^{-1}$ . Absorbers were made of mosaics of foil fragments, with average area densities of about  $12 \text{ mg cm}^{-2}$  of natural Fe and large fractional thickness variations. Transmission Mössbauer spectra were collected using a Ranger MS-1200 spectrometer running in constant acceleration mode. This spectrometer features optimization of the drive signal under computer control which was used to produce an accurate triangular-velocity source motion. Spectra contained  $(1-10) \times 10^9$  counts. Prior to computer fitting, spectra were folded about the zero-velocity channel and summed to eliminate variations in the background counting rate that depend on solid angle. All spectra exhibited a single, broadened, absorption dip of  $\sim 10\%$  depth with unresolved structure due to point defects, as illustrated in Fig. 2 for the equiatomic sample. The lines drawn on the figure indicate intensities of spectral components obtained from a model fit described below.

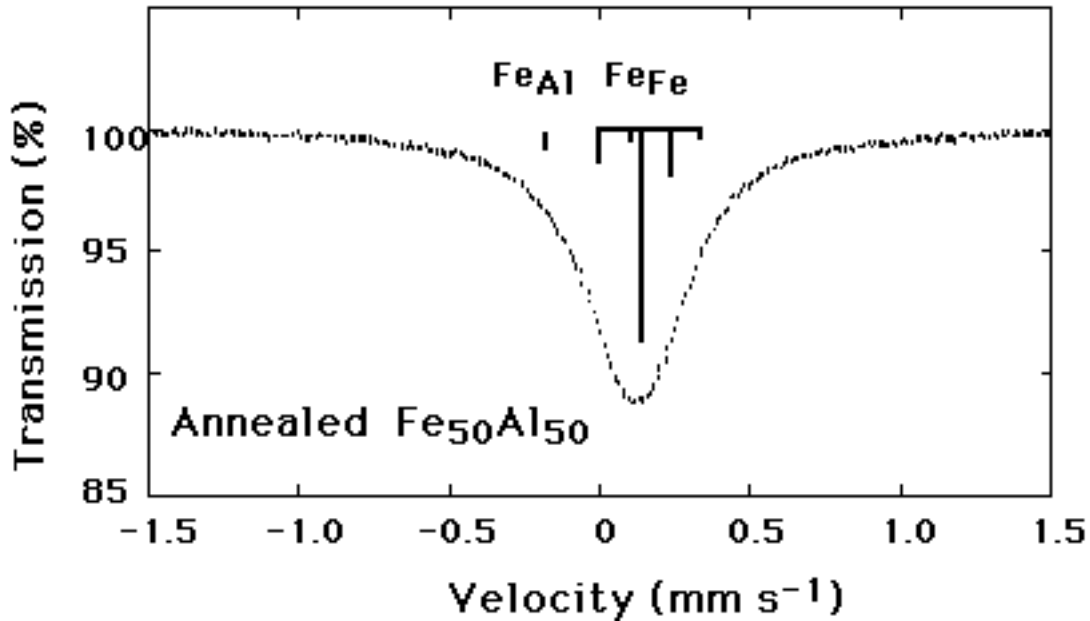


*Figure 2.* Mössbauer spectrum of annealed FeAl. Lines drawn show intensities of spectral components fitted using a local environment model described in the text.

### Method of Analysis

Spectra were analyzed for seven annealed samples with iron concentrations  $c_{\text{Fe}}$  in the range 47-53 at.%. The spectra were fitted with superpositions of absorption lines calculated according to two different local-environment models. Both models shared the following assumptions: (1) Samples are homogeneous, single-phase B2 material. (Possible presence of a second phase below  $\sim 49$  at.% Fe [1] was ignored.) (2) The monopole interaction (isomer shift)  $\delta$  for probe atoms on either sublattice depends on the numbers and types of defects within the nearest two atomic shells. (3) A defect produces

a shift in  $\delta$  depending on the type of defect and its distance from the Fe probe (or shell number).. (4) Shifts due to more than one nearby defect are linearly additive. (5) Recoilless fractions for all sites are equal (so that area fractions are proportional to site fractions.) (6) Point defects are uncorrelated in space, so that the intensities of the different spectral components can be expressed as binomial probabilities in terms of the mole fractions of the different point defects. (7) Quadrupole interactions may be neglected. (7) Lineshapes of discrete lines are adequately approximated by the Lorentzian profile. (8) Resonant self-absorption can be accounted for by a uniform, broadened linewidth for all discrete lines.

We assume that the samples contain structural defects (either  $V_{Fe}$  or  $Fe_{Al}$ , depending on the deviation from stiochiometry), and additional defects due to lattice disorder. The two models differ in the assumptions made about the type of lattice disorder, as follows:

Model A: Triple-defect disorder. As in a recent x-ray study,[1] it is assumed that only  $V_{Fe}$  or  $Fe_{Al}$  defects are present as disorder defects. To preserve the proportions of the constituent elements, this means that mole fractions of the extra disorder defects are constrained to be in the ratio  $c(V_{Fe}):c(Fe_{Al})= 2:1$ . The combination of two vacancies and an antisite atom is known as a triple-defect. Thus, the overall mole fractions of the defect species are not independent, but obey the constraint equation  $c(Fe_{Al}) - 0.5 \cdot c(V_{Fe}) = c_{Fe} - 0.5$ , in which  $c_{Fe}$  is the overall mole fraction of Fe in the sample. Under Model A, assumption (2) above implies that four shifts can be fitted: for the majority  $Fe_{Fe}$  probes these are the shifts due to an  $Fe_{Al}$  defect in the first shell or a  $V_{Fe}$  defect in the second shell, and for the minority  $Fe_{Al}$  probes, there are the shifts due to a  $V_{Fe}$  defect in the first shell or an  $Fe_{Al}$  defect in the second shell. Assumptions (2-4) imply that the monopole interaction  $\Delta(Fe_{Fe};m,n)$  of an  $Fe_{Fe}$  probe having  $m$  first-neighbor  $Fe_{Al}$  defects and  $n$  second-neighbor  $V_{Fe}$  defects is given by

$$\Delta(Fe_{Fe};m,n) = \Delta(Fe_{Fe};0,0) + m \cdot \delta_1(Fe_{Al}) + n \cdot \delta_2(V_{Fe}), \quad (1)$$

in which  $\delta_1$  and  $\delta_2$  are the shifts due to defects in the first and second shells. A similar expression applies for  $Fe_{Al}$  probes. This method of fitting is well known from other studies. [3]

Model B: Antisite-atom disorder. It is assumed under this model that additional disorder defects are present as equal numbers of  $Fe_{Al}$  and  $Al_{Fe}$  antisite-defects, in which case it can be shown that  $c(Fe_{Al}) - c(Al_{Fe}) - 0.5c(V_{Fe}) = c_{Fe} - 0.5$ . Assumption (2) implies that six shifts could be fitted, due to  $Fe_{Al}$ ,  $Al_{Fe}$  and  $V_{Fe}$  defects in the first or second neighbor shells of the two types of probes. To reduce the number of fitting parameters, we made the further assumption that the shift due to a  $Fe_{Al}$  defect in the first shell of an  $Fe_{Fe}$  probe would be the negative of the shift due to an  $Al_{Fe}$  probe in the first shell of an  $Fe_{Al}$  probe, and similarly for complementary antisite defects in the second shell. This amounts to the approximation that the two antisite defects have defect charges of opposite sign.

Monopole interactions for  $^{57}\text{Fe}$  probes without nearby defects on the two sublattices,  $\Delta(\text{Fe}_{\text{Fe}};0,0)$  and  $\Delta(\text{Fe}_{\text{Al}};0,0)$ , were fitted without constraints. Preliminary fitting showed that it was not possible to obtain stable, reliable values for all other parameters by freely fitting because of poor signal resolution. It therefore became necessary to adopt reasonable physical constraints, as described below. Fitted parameters included the (broadened) linewidth  $\Gamma$ , the total spectral area, the monopole interactions for defect-free sites, the shifts caused by the relevant defects of each type and in each shell, and the mole fractions of the defects. Only configurations having a probability greater than 0.01% were included in the computer fitting in order to reduce computation time; with this restriction, typically about 25 configurations were included in the fits.

To reduce numerical instability in the fits, spectra were alternately fitted with  $\Gamma$  fitted and the  $\delta$ 's fixed, and then with the  $\delta$ 's fitted and  $\Gamma$  fixed. Fitted values of  $\Gamma$  for the seven spectra were in the range 0.33-0.36 mm s<sup>-1</sup>. The excess width over the zero-extrapolated absorber width, about 0.08 mm s<sup>-1</sup>, is attributed to the absorber thickness and possibly to smaller shifts due to defects beyond the second shells. On the sides of stoichiometry where  $\text{V}_{\text{Fe}}$  or  $\text{Fe}_{\text{Al}}$  defects have low mole fractions, it was necessary to constrain the  $\delta$ 's to values fitted on the other side of stoichiometry, where mole fractions are larger. The constrained parameters were also checked for consistency by freely fitting them. This procedure led to stable fits, a consistent set of shift parameters, and values of the goodness-of-fit parameter  $\chi^2$  all in the range 1.0-2.0. Better fits were obtained using Model A than Model B, as illustrated in Figure 3, which shows values of  $\chi^2$  from fits of all seven samples. As can be seen,  $\chi^2$  is significantly better for fits using Model A for all samples except the one with 48 % Fe. We conclude that Model A represents the data better and in the following report results only from using that model.

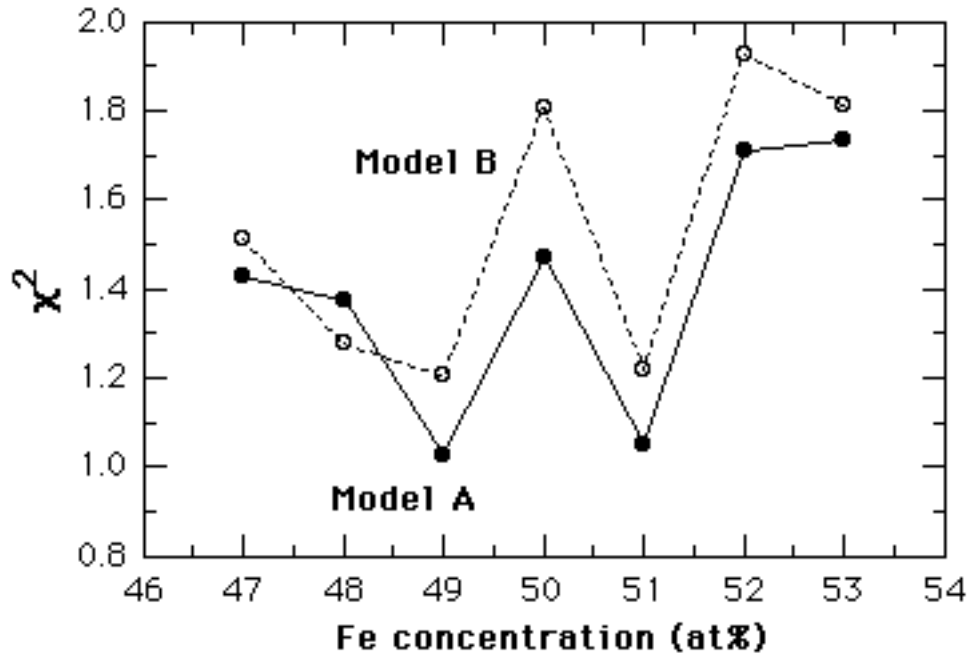


*Figure 3. Goodness-of-fit parameters from fits of seven FeAl samples using Models A and B.*

### Results for Annealed FeAl

**A. Monopole interactions.** Monopole interactions with respect to Fe in alpha-Fe metal of defect-free  $\text{Fe}_{\text{Fe}}$  and  $\text{Fe}_{\text{Al}}$  probes obtained using Model A are drawn as a function of composition in Figure 4. At the 50:50 composition, the shifts are about  $+0.27$  and  $-0.03$   $\text{mm s}^{-1}$ , with respect to  $^{57}\text{Fe}$  in alpha-Fe metal. The monopole interaction for the  $\text{Fe}_{\text{Fe}}$  probes is much more accurately defined because they are much more numerous over the concentration range studied. It can be seen that the interactions at both sites gradually become more positive as  $c_{\text{Fe}}$  increases; the reason for this is unclear but may involve smaller shifts due to defects in shells further away than the two considered here. The  $\text{Fe}_{\text{Al}}$  site, having 8 Fe near-neighbors in the perfect B2 structure, like Fe in alpha-Fe metal, is observed to have the same monopole interaction as Fe in alpha-Fe. The  $+0.27$   $\text{mm s}^{-1}$  interaction for the  $\text{Fe}_{\text{Fe}}$  site, surrounded by 8 Al near-neighbors, can be compared with  $0.57$   $\text{mm s}^{-1}$  for dilute Fe impurities surrounded by 12 Al neighbors in Al metal.[4] Other recent measurements made on FeAl samples near the 50:50 composition exhibit qualitatively similar broadened absorption dips [5, 6] but have not been analysed in the way we have here.

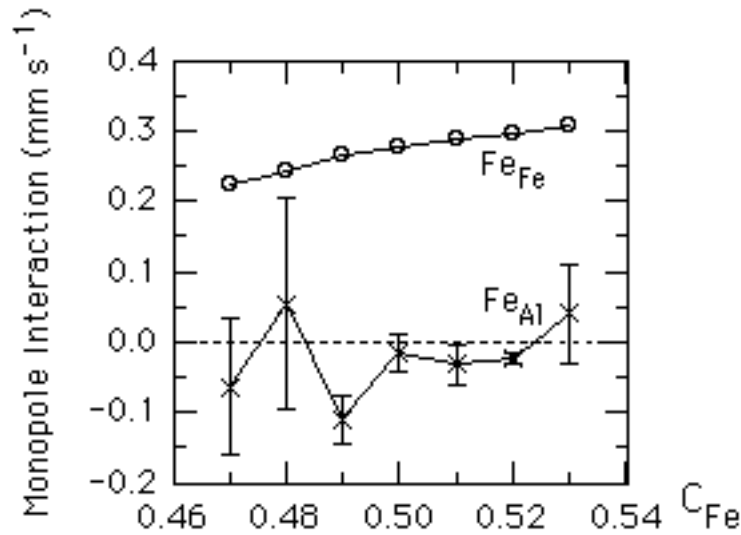


*Figure 4. Monopole interactions of defect-free  $Fe_{Fe}$  and  $Fe_{Al}$  sites in  $FeAl$ , as a function of sample composition, measured with respect to iron metal.*

**B. Defect-induced shifts.** Mean values of the defect-induced monopole-interaction shifts obtained from the analysis using Model A are listed in Table 1. From the table it can be seen that both  $Fe_{Al}$  and  $V_{Fe}$  defects induce negative shifts when in the first shells of Fe probes and positive shifts when in the second shells. Such an oscillatory dependence on distance might arise from screening of the coulomb interaction of the charge defect. The  $-0.31 \text{ mm s}^{-1}$  shift due to a near-neighbor vacancy happens to be the same as the shift for a vacancy next to an Fe probe in Al [4], but this appears to be a coincidence without significance.

*Table 1. Monopole interaction shifts due to defects in  $FeAl$ .*

Defect	Shell number	Probe site	Shift ( $\text{mm s}^{-1}$ )
$Fe_{Al}$	1	$Fe_{Fe}$	-0.134(6)
	2	$Fe_{Al}$	+0.06(17)
$V_{Fe}$	1	$Fe_{Al}$	-0.31(5)
	2	$Fe_{Fe}$	+0.086(5)

Fitted peak velocities and intensities corresponding to the principal probe-defect configurations which were fitted for the 50:50 alloy are indicated on Fig. 2. The small peak farthest to the left corresponds to minority  $Fe_{Al}$  probes without defects in the first two shells. The five peaks on the right correspond, from left to right, respectively, to  $Fe_{Fe}$  probes having  $(m,n) = (1,0), (1,1), (0,0), (0,1),$  and  $(0,2)$  defects in the first and second neighbor shells, respectively.

Are the shifts and monopole interactions consistent? For an  $\text{Fe}_{\text{Fe}}$  probe, replacement of the 8 first-neighbor Al atoms by Fe should lead to a local environment like in alpha-Fe metal. Multiplication of the shift due to a single  $\text{Fe}_{\text{Al}}$  defect,  $-0.14 \text{ mm s}^{-1}$ , by 8 leads to an overall shift of  $-1.1 \text{ mm s}^{-1}$ , much larger than the observed difference in interactions of  $-0.27 \text{ mm s}^{-1}$ . However, the concentration dependence of the monopole interaction for the  $\text{Fe}_{\text{Fe}}$  site shown in Fig. 4 is such as to cause an increase in the interaction by about  $+0.8 \text{ mm s}^{-1}$  if one extrapolates from 50% Fe to 100% Fe, which when added to  $-1.1 \text{ mm s}^{-1}$  yields  $-0.3 \text{ mm s}^{-1}$ , in excellent agreement with  $-0.27 \text{ mm s}^{-1}$ . Thus, the interactions, defect-induced shifts and concentration dependences appear to be internally consistent.

**C. Defect concentrations.** Fitted defect mole fractions are shown as a function of composition in Figure 5. In the figure, curves *a* and *b* represent mole fractions expected if only structural defects needed to accommodate deviations from stoichiometry are present ( $V_{\text{Fe}}$  or  $\text{Fe}_{\text{Al}}$ ) whilst the data points represent total mole fractions of each defect, including additional contributions from lattice disorder.

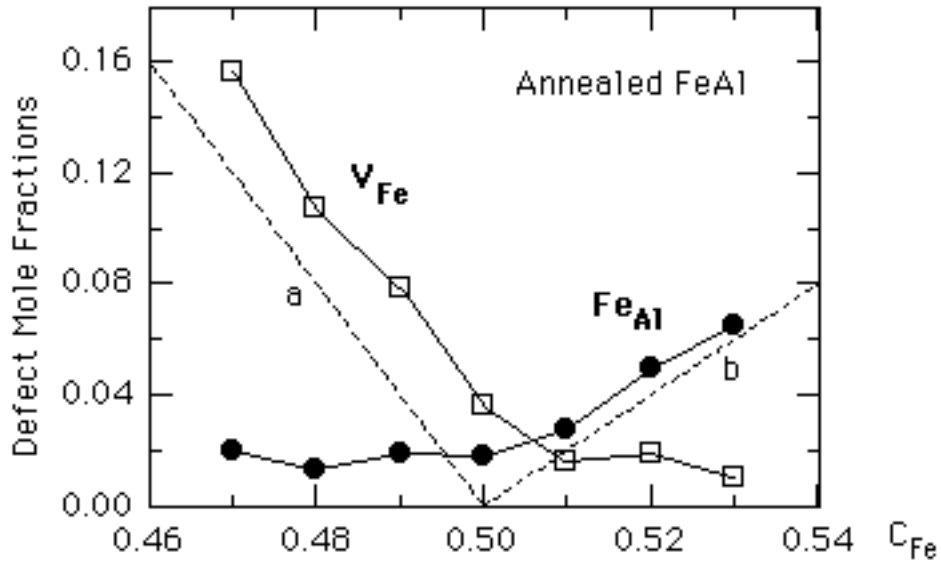


*Figure 5 Mole fractions of  $V_{\text{Fe}}$  and  $\text{Fe}_{\text{Al}}$  defects in annealed FeAl.*

As can be seen, an excess contribution to defect concentrations attributed to disorder is observed to be present over the entire range of compositions studied. The excess concentration of  $\text{Fe}_{\text{Al}}$  is about 2 at.% for 47-50 at.% Fe, decreasing to about 0.5 at.% as one passes to the Fe-rich side of stoichiometry. Thus, Fe-rich alloys are observed to be better ordered than Al-rich alloys for the annealing treatment employed here.

There is good qualitative agreement between defect concentrations determined here and those recently reported from the x-ray measurements by Xiao and Baker [1] but the

excess concentrations observed in the present work are almost a factor of two greater. For example, at the 50:50 composition, mole fractions read from Fig. 7 in Ref. 1 are 1% and 2.7%, respectively, for  $\text{Fe}_{\text{Al}}$  and  $\text{V}_{\text{Fe}}$  defects, whereas they were observed to be 1.8(1)% and 3.6(1)% in the present study. The reason for this discrepancy is unclear. It might possibly be due to small differences between annealing procedures used here and in ref. [1], but more likely it is due to limitations in one or other of the methods of analysis. Certainly in the present work the analysis of unresolved spectral components is pushed about as far as possible.

### Summary

Mössbauer spectroscopy was used to characterize point defects in annealed FeAl using a local environment model. The model yielded a consistent set of monopole interactions and defect-induced isomer shifts. From fits to the model, defect concentrations were obtained that are in good qualitative agreement with other measurement. Experiments to characterize defects and measure defect concentrations in quenched or mechanically-milled samples of FeAl are currently underway. Those sample treatments are likely to generate other elementary defects,  $\text{V}_{\text{Al}}$  and  $\text{Al}_{\text{Fe}}$ , which were not observed in this study. The present study sets the stage for analysis of measurements on such samples. The shift values obtained in the present study will be used as a starting point in that analysis, and we plan to develop models for analysis which are generalizations of the two models considered in the present study.

### Acknowledgment

This work was supported in part by the National Science Foundation under grant DMR 93-13702 (metals program).

### References

---

1. Xiao, H. and Baker, I., *Acta Metall. Mater.*, 43 (1995) 391.
2. See, for example, J. Fan and G. S. Collins, *Hyperfine Interactions*, 60 (1990) 655.
3. See, e.g., Stearns, M.B., *Phys. Rev.*, 147 (1966) 439.
4. Sassa, K., Goto, H., Ishida, Y., and Kato, M., *Scripta Metall.*, 11 (1977) 1029.
5. Vogl, G. and Sepiol, B., *Acta Metall. Mater.*, 42 (1994) 3175.
6. W. Steiner et al., *Proceedings of the Tenth International Conference on Hyperfine Interactions*, Leuven, Sept. 1995.